J Fluoresc (2015) 25:489–501
DOI 10.1007/s10895-015-1539-8

RAPID COMMUNICATION

Fluorescence Behaviour of an Aluminium Octacarboxy Phthalocyanine - $NaYGdF_4$:Yb/Er Nanoparticle Conjugate

Jessica Taylor · Christian Litwinski · Tebello Nyokong · Edith Antunes

Received: 24 November 2014 / Accepted: 23 February 2015 / Published online: 6 March 2015

Abstract Using a methanol assisted thermal decomposition approach, sphere shaped $NaYGdF_4$:Yb/Er upconversion nanoparticles (UCNPs) were successfully synthesized. The chemical, spectroscopic and fluorescence properties of the UCNPs were fully characterized. Characteristic upconversion fluorescence emissions were produced by the NPs in the green, red and NIR regions and the NPs were also shown to possess paramagnetic properties. The influence of the UCNPs on the spectroscopic and fluorescence properties of an aluminium octacarboxy phthalocyanine AlOCPc was investigated. Covalent conjugation to an AlOCPc resulted in a large blue shift of the phthalocyanine's Q band, which was accompanied by a decrease in the Pc's fluorescence lifetime in DMSO. By combining the phthalocyanine and upconversion nanoparticle, we present a system capable of multimodal imaging, using both the upconversion nanoparticle's and phthalocyanine's emission, and magnetic resonance imaging (as a result of doping the upconversion nanoparticles with Gd^{3+} ions).

Keywords Upconversion nanoparticles · Phthalocyanine · Upconversion nanoparticle fluorescence lifetimes · Upconversion nanoparticle steady state emission · Silica shell · Phthalocyanine conjugate

Electronic supplementary material The online version of this article (doi:10.1007/s10895-015-1539-8) contains supplementary material, which is available to authorized users.

J. Taylor · C. Litwinski · T. Nyokong · E. Antunes
Department of Chemistry, Rhodes University, Grahamstown 6140, South Africa

C. Litwinski
PicoQuant GmbH, Rudower Chaussee 29, 12489 Berlin, Germany

E. Antunes (✉)
Department of Chemistry, University of the Western Cape, Bellville 7535, South Africa
e-mail: ebeukes@uwc.ac.za

Introduction

Phthalocyanines have been used extensively in the dye industry and have found numerous applications in chemical sensing, catalysis, solar cells, medicine and various other industrial initiatives [1–4]. In particular, their utilization as photosensitizers in photodynamic therapy has seen continued research interest through the synthesis of new phthalocyanine compounds as well as new combinations with nanostructures to form nanoparticle conjugates. Photodynamic therapy (PDT) has established itself as a non-invasive medical procedure applied to the treatment of cancer and several other diseases [5]. It utilizes reactive oxygen species (such as singlet oxygen) when a photosensitizer, which has accumulated in the tumour cells, is irradiated with selected frequencies of visible light [5].

The optical properties of phthalocyanines (such as strong absorbance in the near infra-red region) make them good candidates for PDT [5, 6]. However, poor solubility and selectivity, together with the fact that the excitation wavelengths for these molecules are still short enough to be intercepted and absorbed by water and other organic molecules in cells and tissue systems, limits penetration depths and severely restricts the treatment areas of PDT [5, 6].

There are several mechanisms by which this problem may be addressed. Firstly, phthalocyanine molecules may be engineered to possess central metals and peripheral substituents which contribute to the red shifting of the molecule's absorption bands [7]. Secondly, phthalocyanines may be attached to other molecules or nanoparticles which, themselves, can act as carrier platforms for the sensitizer, and which can absorb longer wavelengths and produce emissions which are then able to excite the phthalocyanine molecules via an energy transfer mechanism. Ideal initiators for this kind of "indirect" PDT action are upconversion nanoparticles (UCNPs) since they can act, at the very least, as multimodal imaging and delivery agents. In this work, aluminium octacarboxy

phthalocyanine (AlOCPc) is combined with UCNPs and the fluorescence behaviour of the conjugate is examined.

Upconversion nanoparticles possess the ability to absorb radiation in the infrared region and produce visible or UV region emissions [8, 9]. This process utilizes the absorption of two or more infrared photons whose energy is then combined into a single visible or UV photon, producing a fluorescent emission [8, 9].

In their capacity to act as probes for in vivo fluorescence imaging and sensing, UCNPs may be combined with a variety of other molecules in order to create highly fluorescent, multi-functional nanoprobes and drug carriers. One area, which has stimulated some research interest in the last 7 to 8 years, is the application of UCNPs to photosensitizers.

The attachment of photosensitizers to UCNPs has been facilitated utilizing both covalent and non-covalent approaches and usually requires modification of the nanoparticle surface. Polyethylenimine, N-succinyl-N'-octyl chitosan and mesoporous silica are commonly used to alter nanoparticle surfaces. A wide variety of photosensitizer molecules have been employed in conjunction with UCNPs including: a runthenium (II) complex [10], rose Bengal [11], tetraphenyl porphyrin [12, 13], merocyanine 540 [14, 15], chlorin e6 [16–18], hematoporphyrin [19], pyropheophorbide [20], methylene blue [21] as well as three different phthalocyanines including: aluminium tetracarboxy phthalocyanine (AlTCPc) [22], dihydroxy silicon phthalocyanine ($(OH)_2$SiPc) [19] and unsubstituted zinc phthalocyanine (ZnPc) [23–25], with ZnPc being the most studied. In some instances the $NaYGdF_4$ unit is incorporated into a core shell structure with other inorganic crystal species. Still other studies have utilized additional dopants (e.g., manganese). These studies have also been reviewed in more detail elsewhere [26]. For the purposes of this work, a covalent conjugation approach was utilized in order to observe any spectroscopic changes resulting from the addition of UCNPs to phthalocyanines. Conjugation was facilitated by the addition of a 3-aminopropyl triethoxysilane (APTES) functionalized silica shell to the nanoparticle surface. Here we attempt to examine any possible changes in Pc absorbance, fluorescence lifetime and fluorescence quantum yield values arising from the combination of the Pc (AlOCPc) and Er^{3+} activated $NaYGdF_4$ upconversion nanoparticles. Covalent grafting to UCNPs using a tetracarboxy AlPc derivative has been undertaken elsewhere [22]. The octacarboxy AlPc (AlOCPc) used in this work has not been studied in conjunction with a $NaYGdF_4$:Yb/Er@Si@APTES UCNP before, to the best of our knowledge.

The PDT activity of UCNP-Pc conjugates in mouse bladder cancer cells (MB49) using a Zn (II) phthalocyanine photosensitizer has been reported [24]. Uptake of the nanoconjugate into cells was found to be dependent on nanoparticle concentration and time [24]. A recent study has also demonstrated the potential for use of multifunctional UCNPs for both magnetic resonance imaging (through the inclusion of gadolinium in the nanocrystal) and photodynamic therapy (utilizing an aluminium tetracarboxy phthalocyanine (AlTCPc)) [22].

Whilst the use of upconversion nanoparticles as photosensitizer excitation and delivery platforms appears to be achieving some success, one significant challenge, experienced in several studies, is the highly inefficient loading of photosensitizer molecules which adsorb onto the functionalized nanoparticle surface or are encapsulated in mesoporous silica shells. A recent study has presented surface functionalized upconversion nanoparticles which are covalently linked to Rose Bengal photosensitizer molecules. This covalent conjugation approach was shown to significantly improve photosensitizer loading, energy transfer and singlet oxygen quantum yields [11]. The covalent incorporation of AlTCPc inside the silica shells of a $NaGdF_4$:Yb,Er/$NaGdF_4$ UCNP has also been reported [22]. The authors described the synthesis of a $NaGdF_4$:Yb,Er core coated with a $NaGdF_4$ shell followed by further encapsulation with silica where an AlTCPc was embedded in the silica shell [22].

Our work reports on the first covalent conjugation of an octacarboxy Al phthalocyanine to a silica coated $NaYGdF_4$:Yb/Er UCNP ($NaYGdF_4$:Yb/Er@Si@APTES). Until now, no studies have examined the effect of this conjugation on the inherent photophysical properties of the phthalocyanine molecule itself in the presence of UCNPs. This work examines the effect of conjugation to upconversion nanoparticles on the photophysical properties of an aluminium octacarboxy phthalocyanine (AlOCPc). The UCNPs employed in this work are $NaYGdF_4$:Yb/Er. Facilitation of the covalent attachment was achieved through functionalization of the nanoparticle surface with a silica shell to give the $NaYGdF_4$:Yb/Er@Si nanoparticle and 3-aminopropyl triethoxysilane (APTES) to form the $NaYGdF_4$:Yb/Er@Si@APTES. The terminal amino group of APTES allowed for covalent linking to the carboxylic group of the AlOCPc via the formation of an amide bond. The central metal (Al) was chosen due to the fact that AlPc derivatives are already in use for PDT [6] and also the fact that metallated octacarboxy phthalocyanines are monomeric in solution as opposed to their tetracarboxy phthalocyanine derivatives [27]. The resulting conjugate was characterised using X-ray diffraction (XRD), transmission electron microscopy (TEM), Fourier transform infra-red (FTIR) and UV visible absorption spectroscopy. Fluorescence lifetimes and quantum yields of the conjugates were also determined for the conjugate and compared to the Pc alone.

Materials and Methods

Materials

Yttrium nitrate hexahydrate, gadolium chloride anhydrous, ytterbium chloride hexahydrate, erbium chloride hexahydrate, ammonium fluoride (NH_4F), 1-octadecene, oleic acid, Igepal CO-520, tetraethoxysilane (TEOS), 3-aminopropyltriethoxysilane (APTES), N-(3-dimethylaminopropyl)-N-ethylcarbodiimide (EDC), N-hydroxysuccinimide (NHS) and unsubstituted zinc phthalocyanine were purchased from Sigma-Aldrich. NaOH pellets were purchased from SAARChem. Ethanol, methanol, cyclohexane, dimethyl formamide (DMF) and toluene were purchased from SAARChem. Uvasol®, dimethyl sulfoxide (DMSO) and toluene were purchased from Merck.

Equipment

Transmission electron microscope (TEM) images were obtained using a Zeiss Libra TEM at 120 kV accelerating voltage. X-ray diffraction was undertaken using a Bruker D8 discover equipped with a LynxEye detector and Cu-Kα radiation source (1.5403 Å, nickel filter). Samples were analysed upon a silicon wafer slide and diffraction data were collected at 2θ values between 10 and 100° using a locked coupled scan with 9381 steps of 0.00959° at a rate of 0.4 s per step and a slit width of 6 mm. Data were analysed using evaluation curve fitting software, EVA (Bruker), and Rietveld refinements were performed using Topas version 4.2 software (Bruker). A Shimadzu UV-2550 spectrophotometer was used to record UV-visible spectra. Samples were analysed in solution utilizing a quartz cuvette with a path length of 1 cm. Steady state fluorescence spectra were recorded on a Varian Eclipse spectrofluorimeter where the samples were analysed in solution utilizing a quartz cuvette with a path length of 1 cm. Phthalocyanine lifetime measurements were undertaken using a time correlated single photon counting setup (FluoTime 200, PicoQuant) and excite the samples with a laser diode (LDH-P-670 with PDL 800-B, PicoQuant GmbH, 672 nm, 20 MHz repetition rate). Fluorescence was detected under the magic angle with a Peltier cooled photomultiplier tube (PMT) (PMA-C-192-N-M, PicoQuant) and integrated electronics (PicoHarp 300E, PicoQuant). A monochromator with a spectral width of about 4 nm was used to select the required emission wavelength band. The response function of the system, which was measured with a scattering Ludox solution (DuPont), had a full width at half-maximum (FWHM) of about 200 ps. All luminescence decay curves were measured at the maximum of the emission peak. The data were analysed with the program FluoFit (PicoQuant). The support plane approach was used to estimate the errors of the decay times. Upconversion lifetime measurements were recorded using a time correlated single photon counting setup with continuous wave (cw) and flash lamp extension (FluoTime300, PicoQuant). Upconversion emissions were induced using a LDH-D-C-980 diode laser (972 nm, 20 mW pulsed mode, 180 mW cw mode, PicoQuant). Steady state emission spectra were obtained under cw excitation while time resolved measurements were performed using the burst mode with a maximum pulse width of 500 ps. Emissions were detected under the magic angle utilizing a PMA-C 192-M-N photomultiplier tube (PicoQuant). Photon counting was done using an integrated TimeHarp 260 NANO Multi-Channel Scaler card (PicoQuant). The emission from the visible to the NIR spectral range were selectively detected using an Omni-λ300 monochromator with two interchangeable gratings (1200 lines/mm blazed at 500 nm for the visible range and 600 lines/mm blazed at 1250 nm for the NIR spectral range) in combination with motorized slits giving a tunable spectral width between 0.1 and 10.4 mm. Fourier transform infrared spectroscopy (FT-IR) was performed using a Perkin Elmer Spectrum 100 ATR FT-IR spectrometer.

Aluminium octacarboxy phthalocyanine, with an axially ligated chloro substituent, (AlOCPc), was synthesized according to literature methods [28].

Fluorescence Quantum Yields and Fluorescence Lifetimes

Fluorescence quantum yields were calculated using the standard comparison method with Eq. 1 [29] where unsubstituted ZnPc was used as a standard in DMSO with Φ_F values of 0.2 [30]. The standard and sample absorbencies at the vibronic band were kept the same and excitation was done using the wavelength of the cross over point between the vibronic bands of the sample and standard absorbance spectra.

$$\Phi_F = \Phi_{Std} \frac{F.A_{Std}.n^2}{F_{Std}.\mathrm{A}.n_{Std}^2} \quad (1)$$

Here, Φ_F is the quantum yield of the sample and Φ_{Std} that of the standard; F and F_{std} represent the area under the fluorescence emission curve for the sample and standard respectively; A and A_{std} refer to the absorbance of the sample and standard and n and n_{Std} are the refractive indices of the sample and standard solutions, respectively.

The fluorescence lifetime refers to the time spent by a system in the excited state, from which decay by fluorescence occurs and is equal to the reciprocal of the sum of the decay constants for all the relaxation processes acting upon the excited state, as illustrated by Eq. 2 [31, 32]:

$$\tau = \frac{1}{(k_f + k_{nr})} \quad (2)$$

where τ refers to the molecular fluorescence lifetime and k_f and k_{nr} represent rate constants for radiative and non-radiative

decay processes respectively. Fluorescence lifetimes are intrinsic, or state properties, and therefore, they are characteristic of a particular fluorophore and independent of its concentration, as well as the excitation wavelength, intensity and time [31, 32]. They are widely used to investigate the radiative and non-radiative decay rates acting on fluorophore excited states, the interaction of these states with the environment (i.e., with solvents), as well as excited state reaction rates. Lifetime measurements were acquired using the time domain technique, known as time correlated single photon counting, and was used extensively in this work.

Synthesis of $NaYGdF_4$:Yb/Er Upconversion Nanoparticles (UCNP)

Upconversion nanoparticles were synthesized utilizing a methanol assisted thermal decomposition approach as described elsewhere [33]. The relative amounts of Ln ions used differed for the different products. Activator dopants were included at 2 mol % (for the total % of rare earth dopants) for Er^{3+}. Yb^{3+} was included at 18 mol % when co-doped with Er^{3+} and Y^{3+}. However, gadolinium (0.04 mmol–0.24 mmol) and yttrium (0.6 mmols–0.4 mmol) concentrations were purposely varied to obtain the 15, 25 and 30 % Gd doped UCNP. Yield: 70–90 mg.

Synthesis of $NaYGdF_4$:Yb/Er Silica Coated Upconversion Nanoparticles (UCNP@Si)

Synthesis of silica coated UCNPs was undertaken using a modified literature method [34]. Oleic acid stabilized UCNPs (79 mg) (synthesized in "Synthesis of NaYGdF4:Yb/Er upconversion nanoparticles (UCNP)" section) were dispersed in 67.5 ml of cyclohexane. Igepal CO-520 surfactant (1.125 ml, 2.5 mmol) was added and the solution was stirred for 10 min. While stirring, 25 % ammonia (0.9 ml, 12.06 mmol) and additional Igepal CO-520 (4.5 ml, 10.2 mmol) were added. The solution was then agitated using sonication for 1.5 h after which it was stirred for 10 min. Lastly, TEOS (0.45 ml, 2.02 mmol) was added and the solution was left to stir for 4 days. Yield: 30–35 mg.

Synthesis of $NaYGdF_4$:Yb/Er Silica Coated, Amino Functionalized Upconversion Nanoparticles (UCNP@Si@APTES)

APTES functionalization of UCNPs was performed using a modified method found in literature [35]. UCNP@Si NPs (30 mg) were washed several times with dry ethanol and toluene, dried, and added to a mixture of DMF (36 ml) and toluene (24 ml). APTES (1 ml) was added dropwise under argon and the solution was left to stir for 24 h. The functionalized particles were collected by centrifugation and washed several times with toluene. Yield: 25–28 mg.

Synthesis of the $NaYGdF_4$:Yb/Er@si@APTES-AlOCPc Conjugate (UCNP@Si@APTES-AlOCPc)

AlOCPc (15 mg, 0.014 mmol) was added to PBS buffer solution pH 7.4 (15 ml). EDC (0.35 g, 1.8 mmols) and NHS (0.172 g, 1.5 mmol) were added to activate the carboxylic groups of the Pc. The reaction mixture was left to stir for 3 h under argon. UCNP@Si@APTES (5 mg) were suspended in PBS buffer solution pH 7.4 (15 ml) and added to the Pc solution. The mixture was allowed to stir for 15 h under argon. The obtained product was precipitated by adding ethanol and collected by centrifugation. The conjugate particles were washed once with NaOH, to remove unconjugated Pc. Yield: 3.5–4.5 mg.

Results

Structural and Photoluminescence Characterisation of the $NaYGdF_4$:Yb/Er Upconversion Nanoparticles (UCNPs)

Synthesis of UCNPs

Using a methanol assisted thermal decomposition approach, the UCNPs were synthesized in the presence of an oleic acid stabilizer [33]. The use of Gd^{3+} doping was employed in order to control nanoparticle size and shape as well as to impart additional functionality through gadolinium's interesting paramagnetic properties [33]. Gd^{3+} ions were doped in at 15 and 30 mol % for the $NaYF_4$:Yb/Er nanoparticles. Doping of Gd^{3+} ions did not exceed a maximum of 30 mol % due to the unfavorable effects of doping at higher concentrations on fluorescence [33]. Gd^{3+} doping did not appear to influence nanoparticle size and shape to the same degree as reaction temperature and the rate of reaction heating. The control of the maximum temperature at 300 °C was found to be important in controlling the morphological characteristics of the nanoparticles.

In order to facilitate covalent attachment to an AlOCPc, the UCNPs were coated with silica and further functionalised with 3-aminopropyltriethoxy silane (APTES). The silica coated and APTES functionalized particles are represented as $NaYGdF_4$:Yb/Er@Si and $NaYGdF_4$:Yb/Er@Si@APTES, respectively. The particles selected for silica coating and further conjugation to an AlOCPc were $NaYGdF_4$:Yb/Er sphere shaped particles which contained a Gd^{3+} concentration of 15 mol %.

Silica coated UCNPs were synthesized by means of a reverse microemulsion method (Scheme 1). Very simply, added

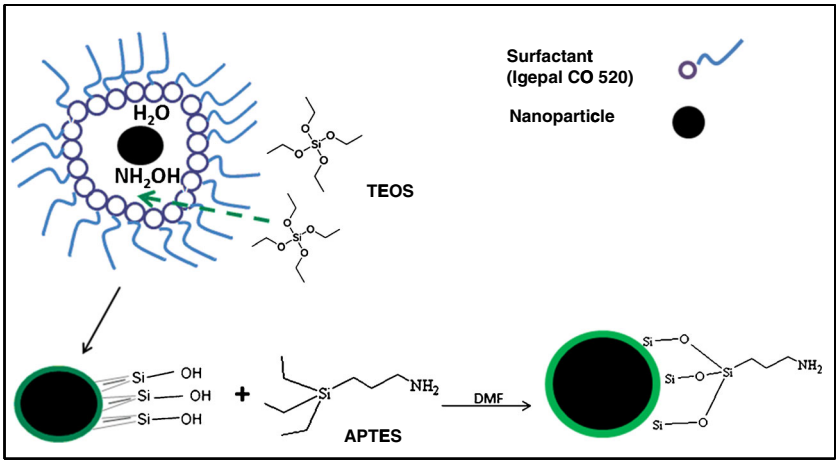

Scheme 1 Simplified representation of the reverse microemulsion synthesis and APTES functionalization of $NaYGdF_4$:Yb/Er@Si UCNPs

surfactant molecules behave as nano sized 'reaction chambers' by enclosing small concentrations of water and ammonia around the oleic acid stabilized UCNPs in a reverse phase micelle [36]. The silica shell is created as tetraethoxysilane (TEOS) becomes concentrated within the micelle and ammonia facilitates the creation of the surface OH groups [36]. The inclusion of nanoparticles within the micelle is reported to involve the initial replacement of surface ligands by surfactant molecules and TEOS [37]. The silica coated nanoparticles can then be further functionalized with APTES by the simple addition of APTES in DMF.

TEM

TEM images of the synthesized $NaYGdF_4$:Yb/Er (Fig. 1a) shows them to be monodispersed, spherical in shape and fairly uniform in size. The white rings surrounding the UCNPs are clearly visible on the TEM micrograph in Fig. 1b, indicating that the UCNPs were successfully coated with silica. From the TEM image, the average thickness of the silica shell was estimated to be around 10 nm. Also shown in the TEM image are small white silicon nanoparticles which are an expected, yet unwanted, by-product of reverse microemulsion. Vigorous washing assisted in the removal of most of the silica nanoparticles; however, to remove them entirely was found to be virtually impossible.

XRD

Powder X-Ray diffraction patterns were obtained for the $NaYGdF_4$:Yb/Er NPs, the $NaYGdF_4$:Yb/Er@Si@APTES NPs and the UCNP-Pc conjugate (Fig. 2). The diffraction patterns for all three samples were well matched to the β phase hexagonal crystal pattern (ICDD card 028-1192). For the $NaYGdF_4$:Yb/ Er@Si@APTES sample (Fig. 2*b*), the broad peak observed at around 2θ=22° is due to the presence of amorphous silica and indicates successful formation of a silica shell on the nanoparticle surface [38], confirming the results obtained from the TEM images.

The average crystallite size of the $NaYGdF_4$:Yb/Er sample was calculated using the Scherrer equation (Eq. 3):

$$d(\text{Å}) = \frac{k\lambda}{\beta\cos\theta} \tag{3}$$

where k is a proportionality constant with a range of values depending upon the crystallite shape and size distribution (typically a spherical particle is assumed with k=0.9), λ is the wavelength for the X-ray source (1.5405 Å for a Cu source), β is the line broadening at full width at half maximum of the selected diffraction peak(s) in radians and θ is the Bragg angle. The peak selected for model fitting using the Scherrer method was the 201 reflection at 2θ=43.5°.

The relatively small size distribution and monocrystalline nature of the samples allowed for a reasonable application of the Scherrer method and despite fairly large (7.7 %) RWP values (weighted profile residuals), the calculated sizes of 27 nm were similar to those obtained using TEM (i.e., 10–27 nm). No real change is observed in the NP's powder diffraction pattern upon silica encapsulation. No change in the NP size was observed either and this is thought to be due to the amorphous nature of the silica, though the TEM unequivocally shows the presence of a shell which is approximately 10 nm thick (as stated above).

IR Spectroscopy of the UCNPs

The presence of surface silica, as well as that of APTES, was also confirmed using infrared spectroscopy (Fig. 3). The uncoated UCNPs (Fig. 3a) possess peaks at 1718 and 2918 cm^{-1} which represent the C=O and CH stretches for oleic acid respectively [39]. A prominent band at around 1070 cm^{-1} represents the Si-O bend (Fig. 3*b*, *c*), while the NH_2 bend at 1653 cm^{-1} (Fig. 3*c*) supports the presence of surface APTES [39].

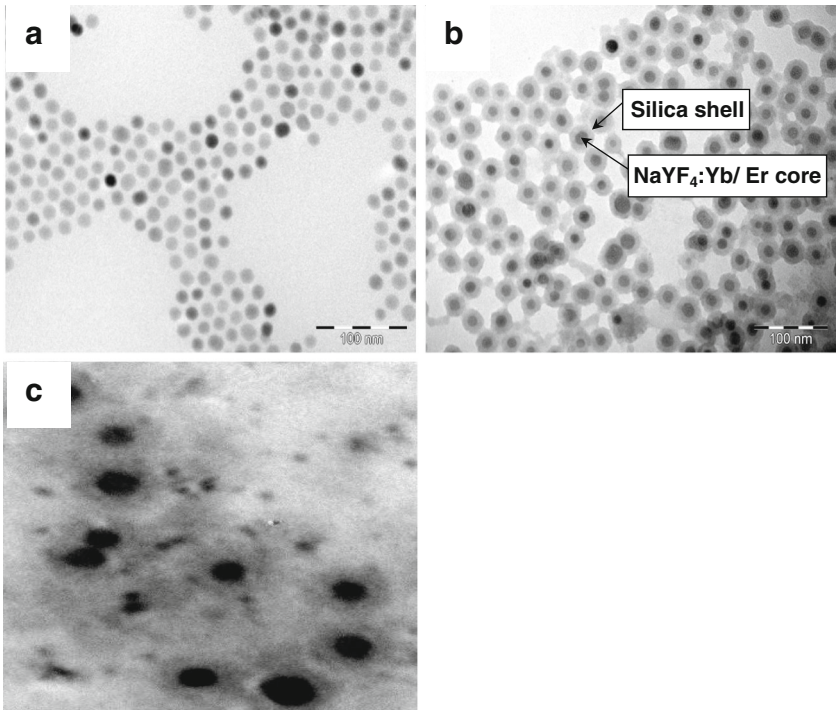

Fig. 1 Transmission electron micrographs of: **a** $NaYGdF_4$:Yb/Er, **b** $NaYGdF_4$:Yb/Er@Si@APTES and **c** the UCNP-Pc conjugate

Steady State and Time Resolved Fluorescence Spectroscopy of the UCNPs

Steady state fluorescence spectroscopy was carried out on the $NaYGdF_4$:Yb/Er samples (10.4 mg) dissolved in toluene (3–4 ml) using 972 nm continuous wave laser excitation. These Er^{3+} activated UCNPs produced emissions at~840, 660, 550 and 530 nm (Fig. 4) and the emissions may be attributed to the $^4S_{3/2}$ - $^4I_{13/2}$, $^4F_{9/2}$ - $^4I_{15/2}$, $^4S_{3/2}$ – $^4I_{15/2}$, $^2H_{11/2}$ – $^4I_{15/2}$ and $^2H_{9/2}$ - $^4I_{15/2}$ transitions, respectively (Fig. 5) [40]. Figure 4 also shows the upconversion emission spectra for silica coated $NaYGdF_4$:Yb/Er spherical nanoparticles. The UC emissions for the silica coated particles were, however, obtained in DMSO. Interestingly, silica coating of the oleic acid stabilized UCNPs resulted in the simultaneous increase and decrease of the 410 and 840 nm emissions respectively, as well as a slight increase in the red emission at 660 nm. These changes are most likely a result of the protection from the environmental quenching effects offered to the UCNP core by the silica shell where population of the higher energy states, at the expense of the lower energy states, is more efficient.

Time resolved fluorescence measurements were acquired for the green, red and NIR emissions of the Er^{3+} activated particles. The analysis of time resolved data for UCNP can be quite complicated in upconversion fluorescence, because population of the energy levels from which fluorescence emissions result from is assisted by the initial population of intermediate states. Generally, the time needed to populate and depopulate excited states is given by a rise and decay components, respectively, in a time resolved fluorescence spectrum. Interpretation of these components varies in the literature.

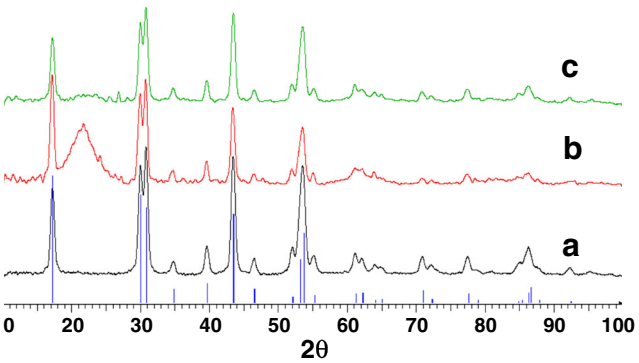

Fig. 2 X-ray diffraction data for: *a*) the oleic acid stabilized $NaYGdF_4$:Yb/Er nanoparticles, *b*) $NaYF_4$:Yb/Er@Si@APTES, *c*) UCNP-Pc conjugate

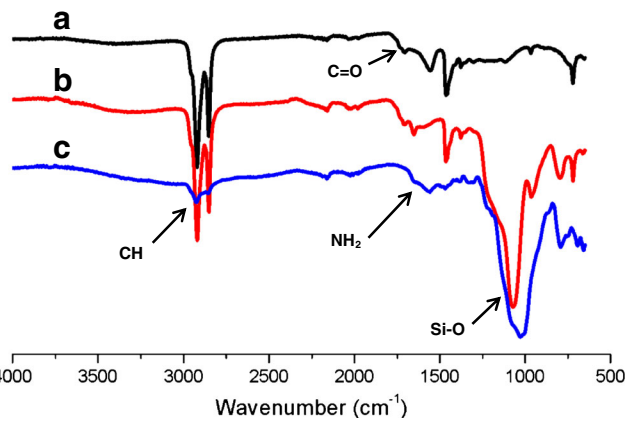

Fig. 3 Infrared spectra of *a*) $NaYGdF_4$:Yb/Er, *b*) $NaYGdF_4$:Yb/Er@Si and *c*) $NaYGdF_4$:Yb/Er@Si@APTES

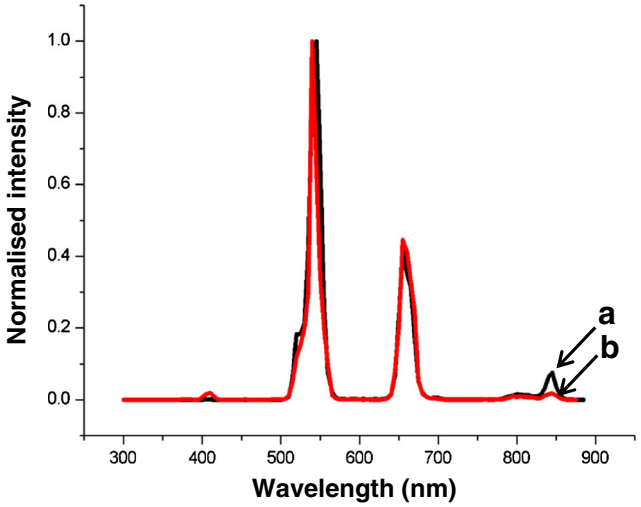

Fig. 4 Steady state UC emission spectra of *a*) $NaYGdF_4$:Yb/Er (in toluene) and *b*) $NaYGdF_4$:Yb/Er@Si (in DMSO) UCNPs. λ_{ex}=972 nm

Authors in one study fitted an entire curve to a kinetic model, reporting two lifetimes that were taken to represent the decay and rise times [41]. The authors maintained that since the long lived intermediate states represent the limiting step in the time mediated population of the higher excited states, the rise time is more reliable in representing the true decay time of the emitting states [41]. Several studies have used the mono exponential fits of the decay portion of the time resolved curve only to report the decay times of the emitting levels only [42], however, while still other researchers have suggested that the application of exponential fitting models is wholly unsuitable

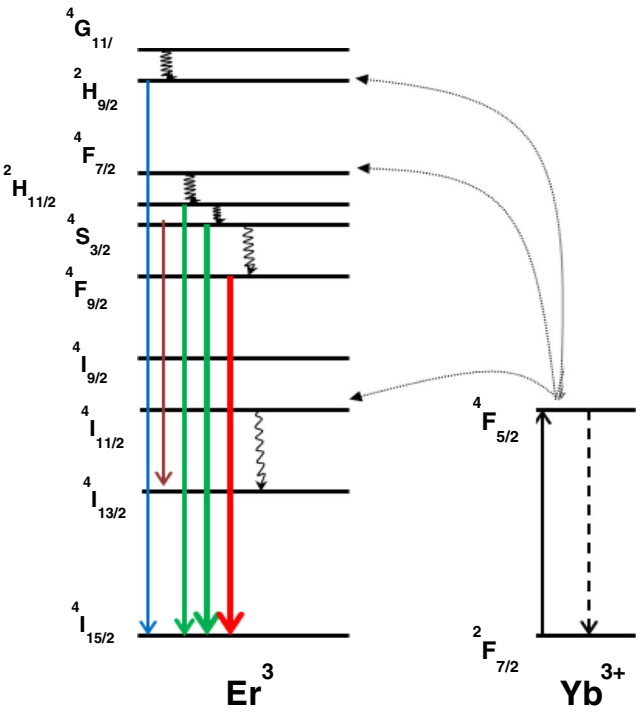

Fig. 5 Electronic transitions giving rise to fluorescent emissions in Er^{3+} ions via Yb^{3+} sensitization. Revised from [40]

[43]. In this work, time resolved emissions were obtained using a high repetition rate, burst mode lasing where multiple laser pulses result in the emission of one photon. The use of burst mode results acts as a barrier to rise time measurements because the rise curve now represents the burst pulses. Therefore, in this work, tail fittings were performed only on the decay curve portion of the time resolved spectrum. Lifetimes were calculated using a multi exponential tail fit equation (Eq. 4) [44]:

$$I_{(t)} = \sum_{i=1}^{n} A_i e^{\frac{-t}{\tau_i}} \tag{4}$$

where n represents the number of exponential components and A_i and τ_i represent the amplitude and decay time of the ith exponential component. A single exponential component was found to best fit the data, with fitting χ^2 values equal to around 1, and all decays could be quantitatively expressed with one lifetime value (Table 1). The statistical fitting errors for the calculated lifetime values were obtained using support plane error analysis and the number of bursts, collection time and bin width parameters were adjusted for each emission in order to yield the smallest fitting errors. In general, increased bin widths and collection times were needed in order to obtain reasonable values for the longer decays. As an example, the decay curves for the green, red and NIR emissions of the $NaYGdF_4$:Yb/Er UCNP sample is shown in Fig. 6, while the lifetime measurements are shown in Table 1.

An increase in fluorescence lifetimes, for both the red and green emissions, was also observed for the silica coated and APTES functionalized nanoparticles (Table 1). While the green emission lifetime experienced only a slight increase of around 10 μs, that of the red emission was found to increase substantially, despite the larger error values. However, it is also possible that these changes may have been induced by the use of DMSO as a solvent. Some studies have highlighted the effect of increasing lanthanide fluorescence lifetimes upon the use of deuterated solvents which are thought to reduce multiphonon loss owing to the lower vibrational energies associated with C-D, as opposed to C-H, bonds [45]. It is possible that DMSO, which possesses fewer C-H groups than

Table 1 UC Fluorescent lifetimes of $NaYGdF_4$:Yb/Er (toluene), $NaYGdF_4$:Yb/Er@Si (DMSO) and $NaYGdF_4$:Yb/Er@Si@APTES (DMSO) UCNPs

	Emissions	τ_F (ms)	Errors (ms)	χ^2
NaYGdF4:Yb/Er	Green	0.093	±0.001	1.005
	Red	0.190	±0.020	1.100
NaYGdF4:Yb/Er@Si	Green	0.103	±0.002	0.974
	Red	0.310	±0.030	1.024
NaYGdF4:Yb/Er@Si@APTES	Green	0.106	±0.004	1.071
	Red	0.240	±0.040	0.951

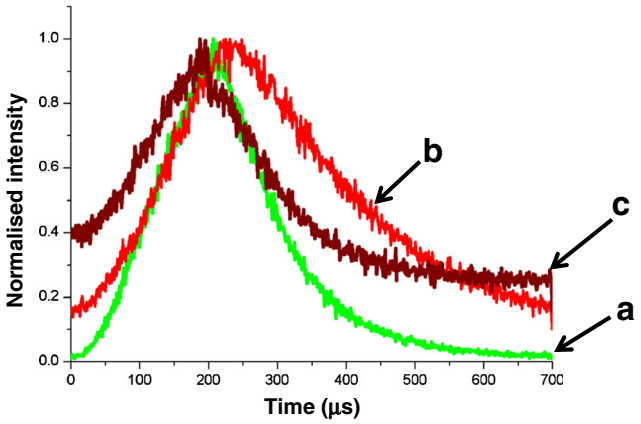

Fig. 6 Time resolved upconversion emission spectra of *green* (*a*), *red* (*b*) and *NIR* (*c*) emissions for the $NaYGdF_4$:Yb/Er spheres. λ_{ex}=972 nm

toluene, may also have contributed to a lower induction of multiphonon loss in this case, thereby increasing the lifetimes and emissions of the particles (Table 1).

Synthesis, Spectroscopic and Photophysical Characterisation of Aluminium Octacarboxy Phthalocyanine

Aluminium octacarboxy phthalocyanine, with a chloro axial ligand, abbreviated AlOCPc (Fig. 7), was synthesized [28] and successfully characterised (see supporting information). Figure 7 shows the absorption, emission and excitation spectra of AlOCPc in DMSO. The peak maxima, 705, 705 and 714 nm for the absorption, excitation and emission spectra respectively, are similar to those obtained in for AlOCPcs in DMSO reported elsewhere [46].

Synthesis, Spectroscopic and Photophysical Characterisation of Aluminium Octacarboxy Phthalocyanine Conjugated to Silica Coated UCNPs (AlOCPc-UCNP)

The AlOCPc–UCNP conjugate was synthesized by adding the amino functionalized UCNPs to AlOCPc in the presence of 1-ethyl-3-(3-dimethylaminopropyl) carbodiimde (EDC) and N-hydroxy succinimide (NHS) coupling agents (Scheme 2). The combined usage of EDC and NHS as coupling agents for the formation of amide bonds has been shown to be significantly more effective than the use of either species in isolation [47]. The conjugation reaction was undertaken in a phosphate buffer solution (PBS) with a pH of 7.4 in order to minimize the effects of acid/ base hydrolysis on amide bond formation. The presence of the amide bond was confirmed using FT-IR (and is discussed in "IR spectroscopy of the AlOCPc-UCNP conjugate)" section.

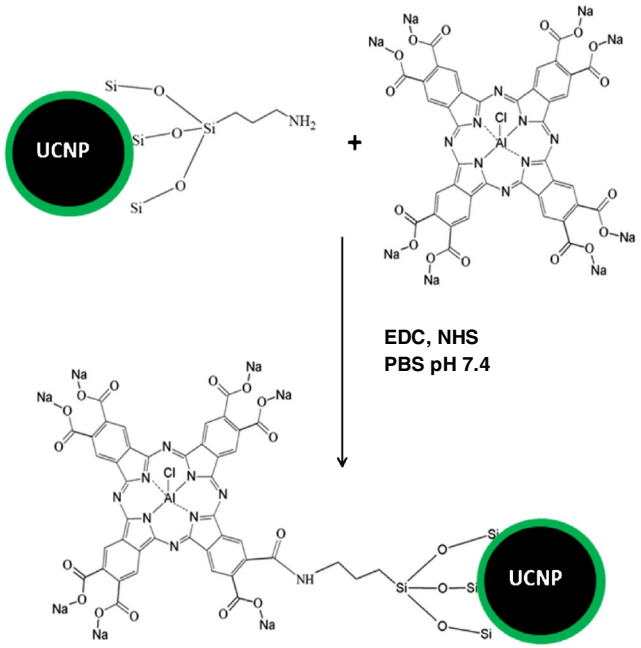

Scheme 2 Synthesis of AlOCPc–UCNP conjugate (scale of NP to Pc not representative)

The TEM images obtained for the conjugate (Fig. 1c) did not clearly show the NPs coated with the phthalocyanine. This is probably due to the fact that that we were unable to find a suitable solvent for the conjugate, thus making spotting the

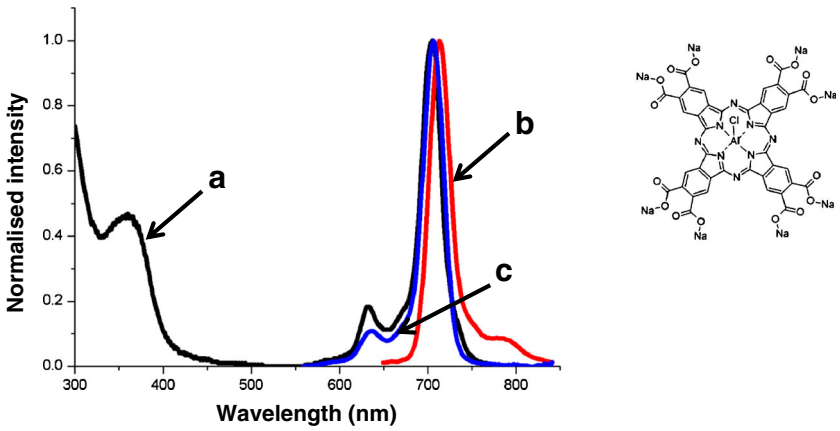

Fig. 7 Normalised absorbance (*a*), emission (*b*) and excitation (*c*) spectra of AlOCPc in DMSO. λ_{ex}=672 nm

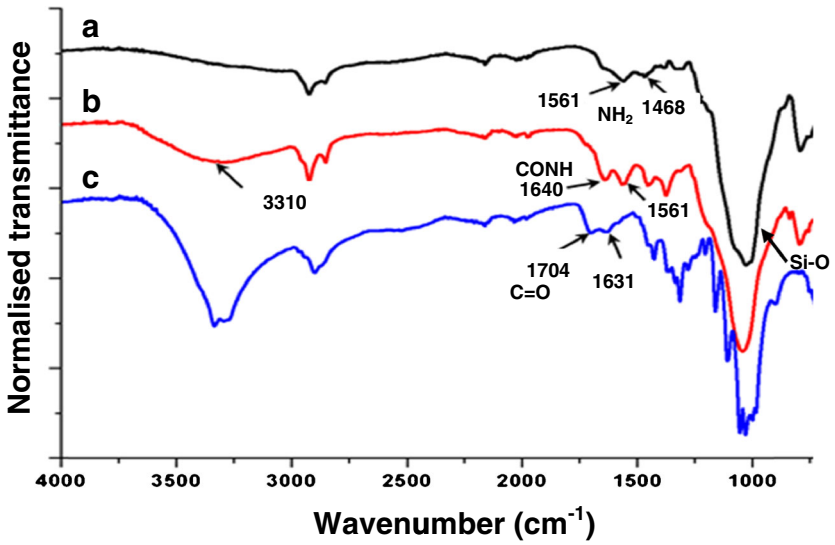

Fig. 8 IR spectra of (*a*) $NaYGdF_4$:Yb/Er@Si@APTES UCNPs, (*b*) AlOCPc-UCNP conjugate and (*c*) AlOCPc

sample on the TEM grid difficult. Dark concentric points with smudges resembling silica shells were observed. However, they do show that the sample underwent a change from the silica coated NPs themselves.

The XRD (Fig. 2*c*) pattern for the AlOCPc–UCNP conjugate shows the diffraction peaks attributed to the UCNP themselves, confirming that the integrity of the NP has not changed upon conjugation. The Pc and silica are both amorphous entities and are therefore not expected to produce sharp peaks.

IR Spectroscopy of the AlOCPc-UCNP Conjugate

The IR spectrum of the amino functionalised UCNP (Fig. 8*c*) displays the characteristic NH_2 group bends at 1561 and 1468 cm^{-1}. The carboxylic acid functional group (C = O) of the AlOCPc is also observed at 1704 cm^{-1} (Fig. 8*c*). Upon conjugation (Fig. 8*b*), this peak was shown to disappear, since it is replaced by a vibration at 1640 cm^{-1} which represents the amide (CONH) functional group. The functionalization of the $NaYGdF_4$:Yb/Er sphere shaped nanoparticles with silica and APTES was discussed in "IR spectroscopy of the UCNPs" section.

Ground State Absorption Spectroscopy and Photophysical Characterisation of the AlOCPc in the AlOCPc-UCNP Conjugate

The Q band in the UV–Vis absorption spectra of the conjugated AlOCPc displayed a striking blue shift of 33 nm from that of the un-conjugated Pc and displayed no peak broadening (Fig. 9). A blue shift as large as 33 nm resulting from conjugation is particularly unusual and such phenomena have not been reported in most studies concerned with the photophysical properties of Pc – NP conjugates. The blue or red shifting of a Pc absorption peak can be directly related to the relative energies of the molecule's HOMO-LUMO levels. As the absorption peak was found to shift to higher energies, one might assume that the energy gap separating the HOMO-

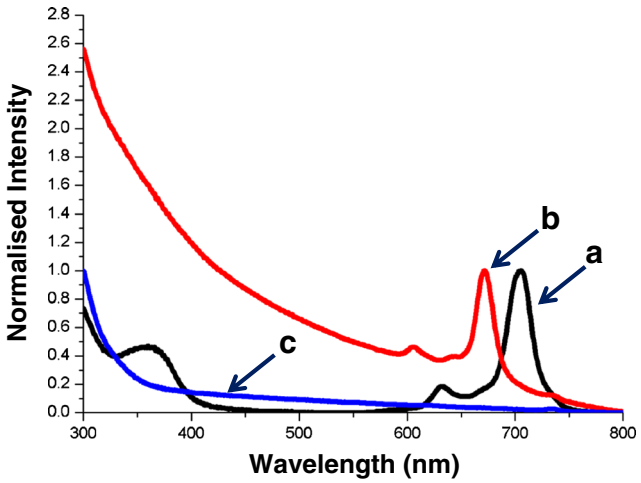

Fig. 9 Absorbance spectra of *a*) AlOCPc, *b*) AlOCPc-UCNP conjugate and *c*) $NaYGdF_4$:Yb/Er@Si@APTES UCNPs in DMSO

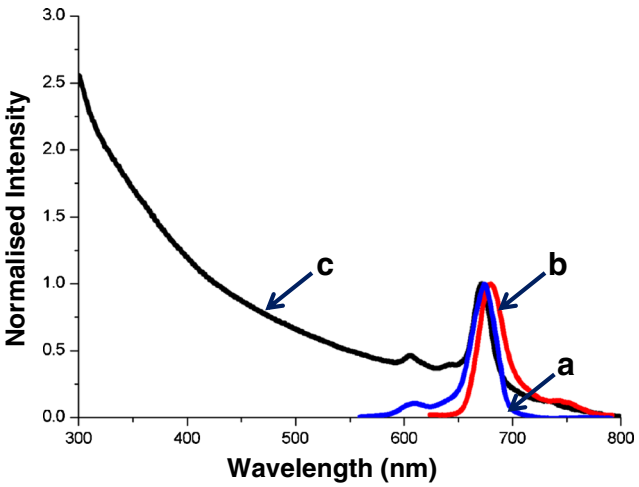

Fig. 10 Absorbance (*a*), emission (*b*) and excitation (*c*) spectra of the AlOCPc-UCNP conjugate in DMSO. λ_{ex}=672 nm

Table 2 Spectroscopic and fluorescence properties of AlOCPc and the AlOCPc-UCNP conjugate in DMSO

	Q_{abs} (nm)	Q_{ex} (nm)	Q_{em} (nm)	τ_F (ns)	χ^2 (abundance)	Φ_f	τ_o (ns)
AlOCPc	705	705	714	5.53±0.02	1.04 (100 %)	0.17	32.53
NaYGdF4:Yb/Er@Si @APTES-AlOCPc	672	674	680	3.17±0.02 0.89±0.03	1.04 (94 %) (6 %)	0.12	26.42

LUMO levels had increased. Red and blue shifting of Q band absorption peaks has been attributed to the electron withdrawing or donating properties of the Pc substituents [48]. In this case, it is possible that the UCNP effectuates a large removal of electron density from the Pc macrocycle, possibly as a result of the high concentration of electronegative F^- atoms in the UCNP core. Presumably, the extent to which the Q band undergoes a blue shift depends upon the number of conjugated substituents through which electron density may be removed. It is possible that the large blue shift reported for this sample may have arisen as a result of several of the carboxylic acid groups of the Pc conjugating to the nanoparticle surface at once, resulting in the Pc macrocycles lying flat against the UCNP surface in a perpendicular orientation. It is possible that the blue shift may have been induced by co-facial aggregation of AlOCPc on the surface of the UCNP; however, this kind of aggregation is usually associated with some degree of peak broadening as well as fluorescence quenching, both of which were not observed [49, 50]. Also, the fact that the blue shift was so large makes co-facial aggregation unlikely to be the cause. In addition, the absorption and excitation spectra of the conjugate were found to overlap, indicating that no change in molecular geometry had occurred upon excitation (Fig. 10).

Conjugation of the AlOCPc also induced significant changes in the fluorescence lifetime whereby the presence of two lifetimes were obtained for the conjugate, one of which, the one in highest abundance, was considerably shorter (3.17 ns) than that of the unconjugated Pc (5.56 ns) (Table 2). A small decrease in the fluorescence quantum yield of the AlOCPc was also observed upon conjugation (Table 2). The decrease in fluorescence lifetimes and quantum yields of the conjugated Pc, as opposed to the Pc alone, may have resulted from several possible phenomena. These include a heavy atom effect [51] as well as the relative orientations of the Pc and UCNP dipole moments. Studies on the photophysical properties of dye molecules linked to gold NPs have shown that dyes attached to the NP surface along their longitudinal axes experience an enhancement of their emitting dipole as a result of the constructive summation of the transition dipole and induced dipole of the dye and NP respectively which are arranged in parallel (Fig. 11) [52]. This emitting dipole enhancement was shown to result in increased fluorescence. In contrast, the anti-parallel arrangement of dye and NP dipole moments associated with the linkage of the dye to the NP surface in a perpendicular or transverse arrangement, i.e., along its shorter axis, was shown to cause a

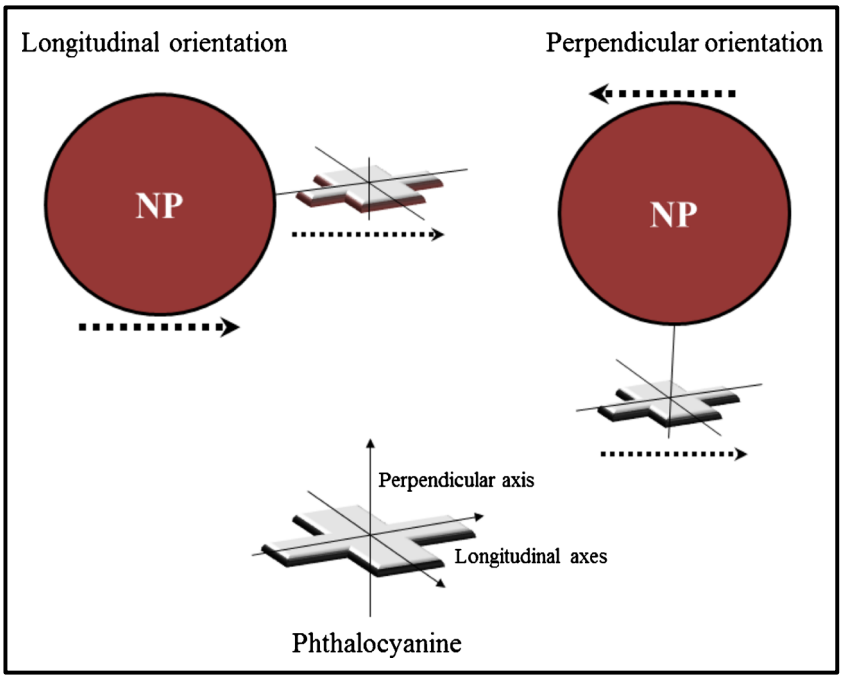

Fig. 11 A diagrammatic representation of the longitudinal and perpendicular arrangements of dye molecules attached to NP surfaces. Transition dipole moments are represented by dotted arrows. Revised from [51]

decrease in fluorescence (Fig. 11) [52]. The effect of distance between the dye and NP surface was also shown to influence the amount of non-radiative energy loss where close proximity of the dye to the NP surface resulted in an increase in lifetime decay [52]. Based on these assumptions, we might assume that the AlOCPc was closely attached to the nanoparticle surface in a perpendicular orientation. However, it should be emphasised, that the above mechanisms were elucidated for conjugations with metallic nanoparticles and the extent to which these same mechanisms operate in NPs consisting of metal salts is unknown. The presence of two lifetimes for the conjugated AlOCPc also suggests that the Pc occupies two different local environments on the surface of the NP [53]. Again, this may involve different orientations of the Pc on the NP surface [53].

In general, it was found that linking the AlOCPc to the UCNP was inefficient, resulting in few covalently linked Pc molecules per UCNP and thus the low absorption peak intensities observed. Also concluded, was that the conjugation of AlOCPc to silica coated UCNPs results in a blue shifted Q band. It is possible that the extent to which the Q band is blue shifted is dependent upon the number of Pc substituents coordinated to the UCNP as well as orientation of the Pc molecule with respect to the UCNP samples.

Fluorescence Properties of UCNPs Conjugated to AlOCPc

In order to examine the effects of conjugation to AlOCPc on the upconversion emissions of the silica coated UCNPs, steady state and time resolved fluorescence measurements were undertaken for the conjugate sample (Fig. 12 and Table 3). The green to red emission peak ratio of the silica coated UCNPs increased upon conjugation to the AlOCPc and this may be a result of energy transfer processes from the UCNP to the AlOCPc. The lifetimes of the conjugated silica coated UCNPs were found to be similar to those of the unconjugated APTES functionalized silica coated UCNPs, indicating that UC emission lifetimes were unaffected by conjugation, presumably as a result of 4f orbital shielding and additional shielding of the metal ions by the silica shell.

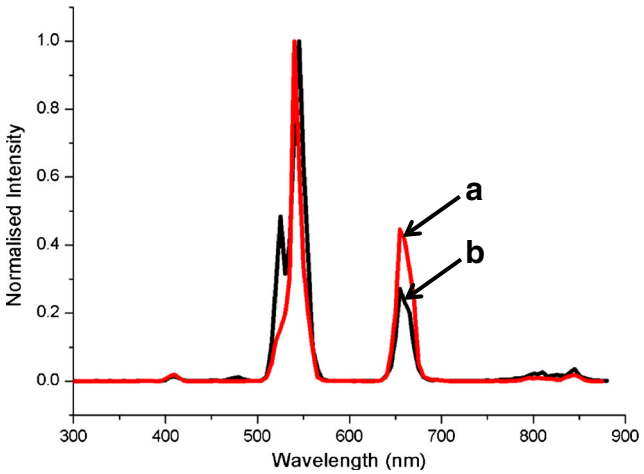

Fig. 12 Upconversion emission spectra of *a*) UCNP@Si and *b*) the AlOCPc-UCNP conjugate in DMSO. λ_{ex}=972 nm

Table 3 Fluorescence lifetimes of AlOCPc-UCNP conjugate and $NaYGdF_4$:Yb/Er@Si@APTES in DMSO. λ_{ex}=972 nm

	Emissions	τ_F (ms)	Errors (ms)	χ^2
AlOCPc-UCNP conjugate	Green	0.103	± 0.002	0.940
	Red	0.220	±0.020	1.100
NaYGdF4:Yb/Er@Si@APTES	Green	0.106	± 0.004	1.071
	Red	0.240	± 0.050	0.951

Conclusion

Sphere shaped $NaYGdF_4$:Yb/Er upconversion nanoparticles were successfully synthesized using a thermal decomposition method and displayed characteristic upconversion fluorescence emissions and magnetic properties (supporting information). EDX (supporting information) and powder diffraction]techniques also suggested that the structural formula of the synthesized UCNPs is likely to be $NaYF_6$. $NaYGdF_4$:Yb/Er nanoparticles were also successfully coated with silica and functionalized with APTES. As expected, silica coating was shown to increase the upconversion emission lifetimes, possibly as a result of decreased surface quenching effects. The effect of conjugating the UCNPs on the spectroscopic and fluorescence properties of the phthalocyanine was also examined. Covalent conjugation to silica coated UCNPs was found to induce significant changes in the spectroscopic and fluorescence properties of the AlOCPc. These changes included a 30 nm blue shift in the Q band absorption peak of the Pc, as well as the appearance of two fluorescence lifetimes, both of which were shorter than that of the unconjugated Pc. These changes are thought to be influenced by the relative orientations of the Pc and NP dipole moments and the number of Pc carboxylic groups bound to the NP surface. The synthesis of the conjugated particles was found to suffer from low yields with low levels of Pc attachment to the UCNP surface. The presence of the Pc appeared to exert no change in the fluorescence lifetimes of the UCNPs, most likely as a result of shielding of the excited state energy levels within the lanthanide activator ions as well as from the host matrix ions. Using 972 nm laser excitation, we were unable to observe any FRET processes between the UCNPs and the conjugated Pc.

Acknowledgments This work was supported through a National Research Foundation CSUR/KFD grant (South Africa), Rhodes University and by the Department of Science and Technology (DST) South Africa through a DST/NRF South African Research Chairs Initiative for the Professor of Medicinal Chemistry and Nanotechnology.

References

1. Kaliya OL, Lukyanets EA, Vorozhtsov GN (1999) Catalysis and photocatalysis by phthalocyanines for technology, ecology and medicine. J Porphyrins Phthalocyanines 3:592–610
2. Trogler WC (2012) In: Mingos DMP, Day P, Dahl JP (eds) Molecular electronic structures of transition metal complexes I. Springer, Berlin Heidelberg, 142:91–118
3. Walter GM, Rudine AB, Wamser CC (2010) Porphyrins and phthalocyanines in solar photovoltaic cells. J Porphyrins Phthalocyanines 14:759–792
4. Allen CM, Sharman WM, Van Lier JE (2001) Current status of phthalocyanines in the photodynamic therapy of cancer. J Porphyrins Phthalocyanines 5:161–169
5. Macdonald IJ, Dougherty T (2001) Basic principles of photodynamic therapy. J Porphyrins Phthalocyanines 5:115–129
6. Bonnett R (1995) Photosensitizers of the porphyrin and phthalocyanine series for photodynamic therapy. Chem Soc Rev 24:19–33
7. Kobayashi N, Furiyama T, Satoh K (2011) Rationally designed phthalocyanines having their main absorption band beyond 1000 nm. J Am Chem Soc 133:19642–19645
8. Haase M, Schäfer H (2011) Upconverting nanoparticles. Angew Chem Int Ed 50:5808–5829
9. Suijver JS (2008) In: Cees Ronda (ed) Luminescence: from theory to applications, WILEY-VHC Verlag GmbH & Co. KGaA, Weinheim, ch. 4, pp. 133–176
10. Guo Y, Kumar M, Zhang P (2007) Nanoparticle-based photosensitizers under CW infrared excitation. Chem Mater 19:6071–6072
11. Liu K, Liu X, Zeng Q, Zhang Y, Tu L, Liu T, Kong X, Wang Y, Cao F, Lambrechts SAG, Aalders MCG, Zhang H (2012) Covalently assembled NIR nanoplatform for simultaneous fluorescence imaging and photodynamic therapy of cancer cells. ACS Nano 6:4054–4062
12. Ungun B, Prud'homme RK, Budijono SJ, Shan J, Lim SF, Ju Y, Austin R (2009) Nanofabricated upconversion nanoparticles for photodynamic therapy. Opt Express 17:80–86
13. Shan J, Budijono SJ, Hu G, Yao N, Kang Y, Ju Y, Prud'homme RK (2011) Pegylated composite nanoparticles containing upconverting phosphors and meso-tetraphenyl porphine (TPP) for photodynamic therapy. Adv Funct Mater 21:2488–2495
14. Idris NM, Gnanasammandhan MK, Zhang J, Ho PC, Mahendran R, Zhang Y (2012) In vivo photodynamic therapy using upconversion nanoparticles as remote-controlled nanotransducers. Nature 18: 1580–1586
15. Zhang P, Steelant W, Kumar M, Scholfield M (2007) Versatile photosensitizers for photodynamic therapy at infrared excitation. J Am Chem Soc 129:4526–4527
16. Park YI, Kim HM, Kim JH, Moon KC, Yoo B, Lee KT, Lee N, Choi Y, Park W, Ling D, Na K, Moon WK, Choi SH, Park HS, Yoon S-Y, Suh YD, Lee SH, Hyeon T (2012) Theranostic probe based on lanthanide-doped nanoparticles for simultaneous in vivo dual-modal imaging and photodynamic therapy. Adv Mater 24:5755–5761
17. Tian G, Ren W, Yan L, Jian S, Gu Z, Zhou L, Jin S, Yin W, Li S, Zhao Y (2012) Red-emitting upconverting nanoparticles for photodynamic therapy in cancer cells under near-infrared excitation. Small 9:1929–1938
18. Wang C, Tao H, Cheng L, Liu Z (2011) Near-infrared light induced in vivo photodynamic therapy of cancer based on upconversion nanoparticles. Biomaterials 32:6145–6154
19. Qiao X-F, Zhou J-C, Xiao JW, Wang Y-F, Sun L-D, Yan C-H (2012) Triple-functional core–shell structured upconversion luminescent nanoparticles covalently grafted with photosensitizer for luminescent, magnetic resonance imaging and photodynamic therapy in vitro. Nanoscale 4:4611–4623
20. Zhou A, Wei Y, Wu B, Chen Q, Xing D (2012) Pyropheophorbide A and c(RGDyK) comodified chitosan-wrapped upconversion nanoparticle for targeted near-infrared photodynamic therapy. Mol Pharm 9:1580–1589
21. Chen F, Zhang S, Bu W, Chen Y, Xiao Q, Liu J, Xing H, Zhou L, Peng W, Shi J (2012) A uniform sub-50 nm-sized magnetic/upconversion fluorescent bimodal imaging agent capable of generating singlet oxygen by using a 980 nm laser. Chem Eur J 18:7082–7090
22. Zhao Z, Han Y, Lin C, Hu D, Wang F, Chen X, Chen Z, Zheng N (2012) Multifunctional core–shell upconverting nanoparticles for imaging and photodynamic therapy of liver cancer cells. Chem Asian J 7:830–837
23. Chatterjee DK, Yong Z (2008) In vivo photodynamic therapy using upconversion nanoparticles as remote-controlled nanotransducers. Nanomedicine 3:73–82
24. Guo HC, Qian HS, Idris NM, Zhang Y (2010) Singlet oxygen-induced apoptosis of cancer cells using upconversion fluorescent nanoparticles as a carrier of photosensitizer. Nanomedicine Nanotechnol 6:486–495
25. Qian HS, Guo HS, Ho PC-L, Mahendran R, Zhang Y (2009) Mesoporous-silica-coated up-conversion fluorescent nanoparticles for photodynamic therapy. Small 5:2285–2290
26. Gu Z, Yan L, Tian G, Li S, Chai Z, Zhao Y (2013) Recent advances in design and fabrication of upconversion nanoparticles and their safe theranostic applications. Adv Mater 25:3758–3779
27. Ozoemena K, Kuznetsova N, Nyokong T (2001) Photosensitized transformation of 4-chlorophenol in the presence of aggregated and non-aggregated metallophthalocyanines. J Photochem Photobiol A Chem 139:217–224
28. Sakamoto K, Ohno E (1997) Synthesis and electron transfer property of phthalocyanine derivatives. Progress Org Coat 31:139–145
29. Fery-Forgues S, Lavabre D (1999) Are fluorescence quantum yields so tricky to measure? A demonstration using familiar stationery products. J Chem Educ 76:1260–1264
30. Ogunsipe A, Maree D, Nyokong T (2003) Solvent effects on the photophysical and fluorescence properties of zinc phthalocyanine derivatives. J Mol Struct 650:131–140
31. Berezin MY, Achilefu S (2012) Fluorescence lifetime measurements and biological imaging. Chem Rev 110:2641–2684
32. Wang F, Han Y, Lim CS, Lu Y, Wang J, Xu J, Chen H, Zhang C, Hong M, Liu X (2010) Simultaneous phase and size control of upconversion nanocrystals through lanthanide doping. Nature 463: 1061–1065
33. Johnson NJJ, Sangeetha NM, Boyer JC, van Veggel CJM (2010) Facile ligand-exchange with polyvinylpyrrolidone and subsequent silica coating of hydrophobic upconverting beta-$NaYF_4$:Yb^{3+}/Er^{3+} nanoparticles. Nanoscale 2:771–777
34. Chang JH, Kang KH, Choi J, Jeong YK (2008) High efficiency protein separation with organosilanes assembled silica-coated magnetic nanoparticles. Superlattice Microst 44:442–448
35. Bhushan B (2010) Introduction to nanotechnology. In: Bhushan B (ed) Handbook of nanotechnology. Springer, Heidelberg, p 2012
36. Koole R, van Schooneveld MM, Hilhorst J, Donega CDM, Hart DCT, van Blaaderen A, Vanmaekelbergh D, Meijerink A (2008) On the incorporation mechanism of hydrophobic quantum dots in silica spheres by a reverse microemulsion method. Chem Mater 20: 2503–2512
37. Park ME, Chang JH (2007) High throughput human DNA purification with aminosilanes tailored silica-coated magnetic nanoparticles. Mater Sci Eng C 27:1232–1235
38. Mayo DW, Miller FA, Hannah RW (2003) Course notes on the interpretation of infrared and raman spectra. Wiley, Hoboken
39. Suyver JF, Grimm J, Veen MKV, Biner D, Kramer KW, Gudel HU (2006) Upconversion spectroscopy and properties of $NaYF_4$ doped with Er^{3+}, Tm^{3+} and/ or Yb^{3+}. J Lumin 117:1–12

40. Zhao C, Kong X, Liu X, Tu L, Wu F, Zhang Y, Liu K, Zeng Q, Zhang H (2013) Li^{+} ion doping: an approach for improving the crystallinity and upconversion emissions of $NaYF_4:Yb^{3+}$, Tm^{3+} nanoparticles. Nanoscale 5:8084–8089
41. Wang J, Wang F, Xu J, Wang Y, Liu Y, Chen X, Chen H, Liu X (2010) Lanthanide-doped $LiYF_4$ nanoparticles: synthesis and multicolor upconversion tuning. Compus Rendus Chimie 13:731–736
42. Schietinger S, AIchele T, Wang H, Nann T, Benson O (2012) Plasmon-enhanced upconversion in single $NaYF_4:Yb^{3+}/Er^{3+}$ codoped nanocrystals. Nano Lett 10:134–138
43. Wlodarczyk J, Kierdaszuk B (2003) Interpretation of fluorescence decays using a power-like model. Biophys J 85:589–598
44. Hebbink GA, Stouwdam JW, Reinhoudt DN, van Veggel FCJM (2002) Lanthanide (III) - doped nanoaprticles that emit in the near-infrared. Adv Mater 14:1147–1150
45. Malinga N, Dolotova O, Bulgakov R, Antunes E, Nyokong T (2012) Synthesis and physicochemical behaviour of aluminium trikis and tetrakis (diaquaplatinum) octacarboxyphthalocynine. Dyes Pigments 95:572–579
46. Jiang L, Glidle A, Griffith A, McNeil CJ, Cooper JM (1997) Characterising the formation of a bioelectrochemical interface at a self-assembled monolayer using X-ray photoelectron spectroscopy. Bioelectrochem Bioenerg 42:15–23
47. Kobayashi N, Ogata H, Nonaka N, Luk'yanets EA (2003) Effect of peripheral substitution on the electronic absorption and fluorescence spectra of metal-free and zinc phthalocyanines. Chem-A Eur J 9: 5123–5134
48. Snow AW (2003) Phthalocyanine Aggregation. In: Kadish KM, Smith KM, Guilard R (eds) The Porphyrin Handbook. Academic, San Diego, pp 129–176
49. Cong F-D, Gao G, Li J-X, Huang G-Q, Wei Z, Yu F-Y, Du X-G, Xing K-Z (2010) Synthesis and aggregation study of optically active tetra-beta-[(S)-2-octanyloxy]-substituted copper and nickel phthalocyanines. J Chem Sci 122:813–818
50. Seybold PG, Gouterman M (1969) Porphyrins: XIII: fluorescence spectra and quantum yields. J Mol Spectrosc 31:1–13
51. Vukovic S, Corni S, Mennucci B (2009) Fluorescence enhancement of chromophores close to metal nanoparticles. Optimal setup revealed by the polarizable continuum model. J Phys Chem C 113: 121–133
52. Kotiaho A, Lahtinen R, Efimov A, Metsberg H-K, Sariola E, Lehtivuori H, Tkachenko NV, Lemmetyinen H (2010) Photoinduced charge and energy transfer in phthalocyanine-functionalized gold nanoparticles. J Phys Chem C 114:162–168
53. McGown LB, Nithipatikom K (2000) Molecular fluorescence and phosphorescence. Appl Spectrosc Rev 35:353–393